Development of ultra-ductile strain-hardening cementitious composites with non-oiled PVA fibers by coupling effect of fly ash and carbon black

Zhigao Yao · Chang Lin · Shuying Xu · Lisha Pan

Abstract Due to its excessively strong bond with cementitious matrices, polyvinyl alcohol (PVA) fibers used in strain-hardening cementitious composites (SHCC) were generally treated with oiling agents, which is expensive. This study developed SHCC with an ultimate strain up to 5.9% by using non-oiled PVA fibers along with high dosages of fly ash and carbon black. The compressive strength of the matrices was controlled within a suitable range from 18 to 96 MPa, by altering the dosages of fly ash and carbon black as well as superplasticiser. The involved PVA fibers were free from any surface treatment and at a volumetric fraction of 2%. The properties of SHCC were characterized by direct tensile test, fiber pullout test and microscopic examination. The experimental results indicated that the coupling effect of fly ash and carbon black enhanced multiple-cracking and strain-hardening behavior under direct tension. It was also indicated that both fly ash and carbon black at sufficient dosages reduced the interfacial interaction between PVA fibers and cementitious matrices, and prevented premature fracture of PVA fibers.

Keywords SHCC · Direct tensile test · Interfacial interaction · Fiber pullout · Bond

Z. Yao · C. Lin (✉) · S. Xu · L. Pan
School of Chemical Engineering and Technology, Hainan University, Haikou 570228, China
e-mail: clin@hainanu.edu.cn

1 Introduction

With a delicate design on their matrices, fibers and the interactions between them, strain-hardening cementitious composites (SHCC) or engineering cementitious composites (ECC) exhibit prominent toughness and ductility with an ultimate strain up to 3% or even higher [1–3]. It has been indicated that SHCC can be used to enhance the anti-impact, durability and self-healing capacity of structures [4–8].

The high toughness and high ductility of SHCC are associated with the strain-hardening and multiple-cracking behavior under direct tension [9, 10]. To achieve this behavior, it is crucial to choose fibers with suitable properties, dimensions, and bond with cementitious matrices. The fibers commonly used in cementitious composites include steel, glass, polypropylene (PP), polyethylene (PE) and PVA fibers [11–15]. PVA fibers are competitive both in price and mechanical performance [2], and have been widely used to develop SHCC [1, 2, 16–18]. Due to their hydrophilic nature, PVA fibers tend to exhibit excessively strong bond with cementitious matrices. As a result, severe fiber surface abrasion and slip-hardening behavior occur during the pullout process of PVA fibers, which leads to reduction in the apparent strength and premature fracture of the fibers [19]. Hence, oil coating and other surface treatment have been designed for PVA fibers to optimize their toughening performance in cementitious matrices [2, 17, 18].

To date, most SHCC have been produced with oiled PVA fibers from Kuraray Co. Ltd. in Japan, involving high costs. In China, the price for non-oiled PVA fibers of similar strength and elastic modulus is about 1/8 that of oiled PVA fibers [20]. It will accelerate the practical application of SHCC in construction industry if non-oiled PVA fibers can be used to produce high-ductility SHCC. Hence, different approaches have recently been explored to enhance the performance of non-oiled PVA fibers in SHCC by redesigning the compositions [20] or tailoring the matrices with new ingredients such as rubber [21]. In the current study, carbon black is used to alter the bond between non-oiled PVA fibers and cementitious matrices containing high-volume fly ash.

Carbonaceous materials such as carbon fibers, graphene nanoplatelets and carbon nanotubes have been incorporated in concrete and cementitious composites to change their mechanical properties and electrical conductivity to enable their self-sensing ability in monitoring structural health [22–25]. Carbon black has been included in SHCC with oil-coated PVA fibers for developing self-sensing ability [24, 25]. While the self-sensing ability resulted from carbon black has attracted attention, its effect on interfacial interactions between PVA fibers and matrices has been neglected. It has been found that residual carbon in fly ash prefers to concentrate on the surface of PVA fibers, and acts as a lubricant that modifies the interfacial bond [26]. Hence, it is plausible to suggest the proper usage of carbon black could optimize the interfacial interaction between non-oiled PVA fibers and cementitious matrices.

The current study aims to provide a new pathway to developing ultra-ductile SHCC with non-oil-coated PVA fibers by carbon black at proper dosages to modify the interfacial interaction between non-oiled PVA fibers and cementitious matrices. The focus is specifically placed on the coupling effect of carbon black and fly ash at different dosages on the tensile properties and interfacial interaction of SHCC with non-oiled PVA fibers.

2 Experimental program

2.1 Materials

The cement is Type PO42.5 from Hainan Landao Environmental Protection Industry Co., Ltd. The fly ash is Class F from Yulian Power Plant in Gongyi City in China. The chemical composition and physical properties of the cement and the fly ash are listed in Table 1. Tap water was used as the mixing water.

Polycarboxylate based superplasticiser from Shaanxi Qin Jian Group Co., Ltd was used. The properties of PVA fibers are given in Table 2. The PVA fiber named as WW40 with a diameter of 40 μm was manufactured by Anhui Wanwei Group Co., Ltd, and was used in making SHCC specimens for direct tensile tests. For the feasibility of conducting fiber pullout test under the laboratory conditions of current investigation, PVA fiber named as TY140 with a diameter of 140 μm was manufactured by Changzhou Tian Yi Engineering Fiber Co., Ltd, and was used in fiber pullout tests. Both PVA fibers are neither oil-coated nor with any other surface treatment. The carbon black was Mitsubishi MA100, with a density of 1800 kg/m^3 and a surface area of 1.1×10^5 m^2/kg.

Table 1 Chemical composition by mass percentage (%) and physical properties of cement and fly ash

	Cement	Fly ash
SiO$_2$	19.25	53.96
Al$_2$O$_3$	6.60	31.14
Fe$_2$O$_3$	3.74	3.86
CaO	58.23	4.01
MgO	3.64	1.01
Na$_2$O	0.30	0.88
K$_2$O	0.52	1.01
TiO$_2$	0.99	1.13
MnO	0.40	–
SO$_3$	3.44	0.72
Loss on ignition (%)	2.18	2.00
Density (kg/m^3)	3110	2170
Surface area (m^2/kg)	476	1137

Table 2 Properties of the fibers

Fiber	Diameter (mm)	Length (mm)	Aspect ratio	Density (kg/m^3)	Tensile strength (MPa)	Elastic modulus (GPa)
WW40	0.040	12	300	1300	1560	41
TY140	0.140	15	107	1300	1200	17

Table 3 Mix proportions[a]

Mix No	Cement	Fly ash	Water	SP[b]	CB	Fiber	W/CM[c]	SP/CM[d]	CB/CM[e]	CB/V_t[f] (kg/m^3) (%)	V_f[g] (%)
F0CB0	1	0	0.21	0.007	0	0.0144	0.21	0.007	0	0	2
F0CB2	1	0	0.21	0.007	0.0010	0.0144	0.21	0.007	0.0011	2	2
F0CB10	1	0	0.21	0.013	0.0054	0.0144	0.21	0.013	0.0055	10	2
F0CB20	1	0	0.21	0.019	0.0109	0.0144	0.21	0.019	0.0110	20	2
F1CB0	1	1	0.42	0.014	0	0.0322	0.21	0.007	0	0	2
F1CB2	1	1	0.42	0.014	0.0024	0.0322	0.21	0.007	0.0012	2	2
F1CB10	1	1	0.42	0.020	0.0122	0.0322	0.21	0.010	0.0064	10	2
F1CB20	1	1	0.42	0.036	0.0247	0.0322	0.21	0.018	0.0122	20	2
F2CB0	1	2	0.63	0.016	0	0.0511	0.21	0.005	0	0	2
F2CB2	1	2	0.63	0.016	0.0037	0.0511	0.21	0.005	0.0012	2	2
F2CB10	1	2	0.63	0.036	0.0190	0.0511	0.21	0.012	0.0064	10	2
F2CB20	1	2	0.63	0.060	0.0385	0.0511	0.21	0.020	0.0128	20	2
F4CB0	1	4	1.05	0.050	0	0.0871	0.21	0.010	0	0	2
F4CB2	1	4	1.05	0.050	0.0065	0.0871	0.21	0.010	0.0013	2	2
F4CB10	1	4	1.05	0.075	0.0328	0.0871	0.21	0.015	0.0065	10	2
F4CB20	1	4	1.05	0.100	0.0661	0.0871	0.21	0.020	0.0130	20	2

[a]All numbers are given in mass ratios to cement, unless otherwise noted

[b]SP refers to superplasticiser

[c]W/CM refers to mass ratio of water to the total cementitious materials including cement and fly ash

[d]SP/CM refers to the mass ratio of superplasticiser to the total cementitious materials including cement and fly ash

[e]CB/CM refers to the mass ratio of carbon black to the total cementitious materials including cement and fly ash

[f]CB/V_t refers to the mass of carbon black in kg per cubic meter volume of the mixture

[g]V_f is fiber volumetric fraction

2.2 Specimen fabrication

The mix proportions are given in Table 3. The dosage of carbon black is given in kg per cubic meter mixture. The dosages under investigation include 2, 10 and 20 kg, presenting low, medium and high dosages, respectively. The dosage of fly ash is expressed as a mass ratio of fly ash to cement (FA/C). The FA/C ratios under question include 1, 2 and 4. The mixture is identified "FxCBy" in which x and y refer the FA/C ratio and the dosage of carbon black, respectively. For

instance, F1CB10 refers to the mixture with a FA/C ratio of 1 and a carbon black dosage of 10 kg/m^3. For specimen fabrication, the superplasticiser was first dissolved in the mixing water, and then the resultant solution was pulled into the flask containing the carbon black powders, followed by ultrasonication for 5 min at 40 kHz to disperse carbon black in water. After the cement and the fly ash were fed into the mixer and dry-mixed for 2 min, the water with dissolved superplasticiser and dispersed carbon black was poured in and mixed for another 3 min. Shortly,

the fibers were gradually added while mixing, the process of which lasted about 3 min.

After mixing for an additional 2 min, the mixture was cast into the molds. All mixtures were highly workable, and only slight shaking by hand was applied for compaction. After 24 h, the specimens were taken out of the molds and stored in a curing chamber where the temperature was 23 ± 2 °C and the humidity was $95 \pm 2\%$. The tests were carried out at the age of 28 days. The specimens were taken out of the curing chamber and placed in room condition for drying one day prior to testing. In the current study, the volume fraction of fibers was consistently 2%.

2.3 Mini-slump flow test

To achieve a similar consistency, trial mixtures without fiber were first tested by mini-slump flow test. In the mini-slump flow test, a fresh mixture was poured into a truncated cone mold which was placed on a level smooth glass plate, followed by vertically lifting up the truncated cone. The mixture spread over the glass surface. The spread value was the average of two orthogonal diameters of the spread. The truncated cone mold is 65 mm in upper inner diameter, 75 mm in lower inner diameter, and 40 mm in height.

2.4 Compressive test

The compressive strength test for plain matrices was carried out on a YAW-2000B electro-hydraulic servo testing machine with a 2000 KN load cell at a load rate of 1.5 KN/s. The specimens were cubic in shape with an edge length of 50 mm. The compressive strength value was obtained by averaging those of at least three specimens in each case.

2.5 Direct tensile test

Dog-bone shape specimens as shown in Fig. 1a were used for direct tensile test. Based on previous studies [16, 27], a setup for direct tensile test as shown in Fig. 1b was adopted. The direct tensile tests were carried out on a WDW-100 T universal testing machine with a 100 KN load cell. Two linear variable differential transformers (LVDT) were used to measure the displacement of the gauge section. The gauge section was 150 mm in length with a rectangular section of 36×20 mm. To facilitate the alignment

and exclude bending moment, the specimen was attached onto the machine by a spherical joint at each end. The load rate was controlled by the crosshead movement at a rate of 0.1 mm/min. At least 3 specimens were tested for each case.

After direct tensile tests, the number of cracks in specimens was counted by a method as in reference [28] and the loaded crack width is calculated by

$$w = \frac{\Delta l}{N} \tag{1}$$

where Δl is the measured deformation value at the peak load in direct tensile test, and N the number of cracks [28]. The residual crack width was measured with an optical microscope.

2.6 Fiber pullout test

As shown in Fig. 2a, the mold for casting specimens for fiber pullout test has a detachable copper plate with a hole at the center for the fiber passing through. Three pieces of rectangular foam boards are used for fiber fixation. One piece with the support from the other two pieces is aligned parallel with the copper plate, as can be seen in Fig. 2a. The PVA fiber is not stiff enough to pierce through the foam board, so the foam board was first pierced by a needle to create a channel for the fiber passing through. The fiber was placed in the mold, passing through the hole of the copper plate and through the foam board. After the fixation of the fiber, the matrix mixture was cast into mold at the other end with a fiber embedded length of 6 mm for all cases. The specimens were demolded from the mold after 24 h and cured at the same condition as for tensile test specimens. The specimens were tested at the age of 28 days. At least 6 specimens were tested for each case.

The geometry of specimens for fiber pullout test is shown in Fig. 2b. The fiber pullout test was carried out on an INSTRON 3343 testing machine with a 1 KN load cell, as displayed in Fig. 2c. To facilitate the gripping and alignment, the free end of the fiber was glued on a piece of square cardboard with the fiber aligned vertically to the edge of the square cardboard, then covered conjunctively with another piece of square cardboard of the same size. The free end of the fiber was aligned with the edge of the square cardboard overlapping that of the rectangular gripping plates of pneumatic grips on the testing machine as shown in
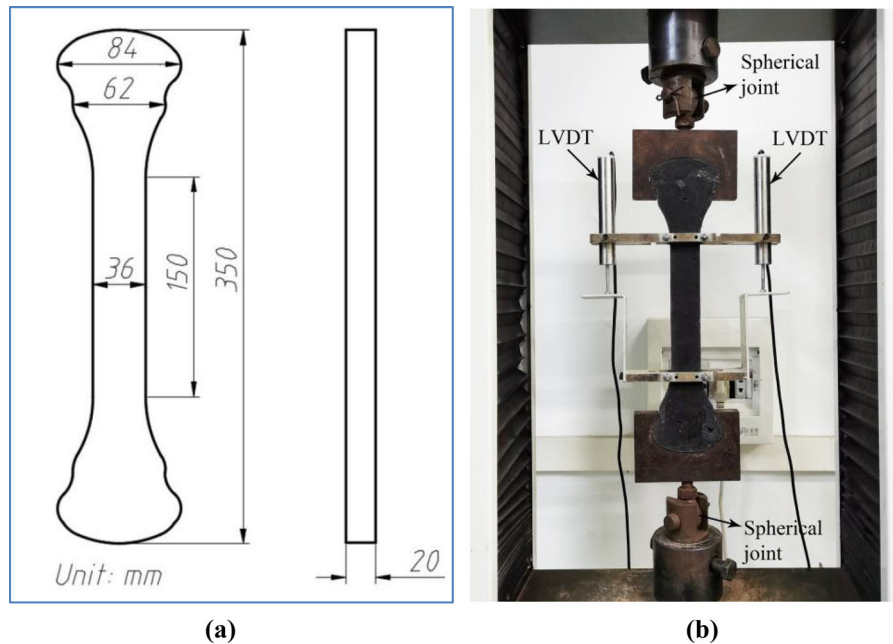
Fig. 1 **a** Geometry of dog-bone specimen; **b** direct tensile test setup

Fig. 2d. The load rate was controlled by the movement of the crosshead at a rate of 0.1 mm/min.

3 Results and discussion

3.1 Flowability

It was observed from trial mixes that adding 2 kg carbon black per cubic meter mixture exhibited little influence on workability. With its dosage increased to 10 or 20 kg/m³, however, carbon black obviously reduced the workability of the mixtures. Hence, a higher dosage of superplasticiser was adopted for the mixtures containing 10 or 20 kg/m³ carbon black to achieve certain workability. All final mixtures of plain matrices displayed similar workability with spread values ranging from 245 to 287 mm in mini-slump flow tests, as listed in Table 4. The dosage of superplasticiser required for the mixtures containing 20 kg/m³ carbon black was more than twice of that for mixtures without or with 2 kg/m³ carbon black. This is probably due to the high surface area of carbon black. The carbon black contains micro- and nanoparticles mostly with spherical shapes as can be seen from its

scanning electron microscopy (SEM) images in Fig. 3a. The specific surface area of carbon black is 1.1×10^5 m²/kg, which is much larger than that of cement and fly ash.

Also, it is likely that the surface of carbon black particles adsorbs superplasticiser and reduces the water-reducing effect of superplasticiser. It was confirmed by comparing the stability of carbon black particles in water. The same amount of carbon black was first dispersed by ultrasonication in water without and with dissolved superplasticiser. After standing still for 5 min, the carbon black particles precipitated in the former case, but suspended in the water in the latter, as presented in Fig. 3b. Due to its surfactant effect, superplasticiser is adsorbed on the carbon black particles and stabilizes the suspension.

3.2 Compressive strength and density

As can be seen in Table 4, the compressive strength of all matrix specimens ranges from 18.7 to 95.1 MPa. According to previous publications [1, 16], this strength range is suitable from designing SHCC with PVA fibers. It is also clear from Fig. 8 that the compressive strength of plain matrices declines with
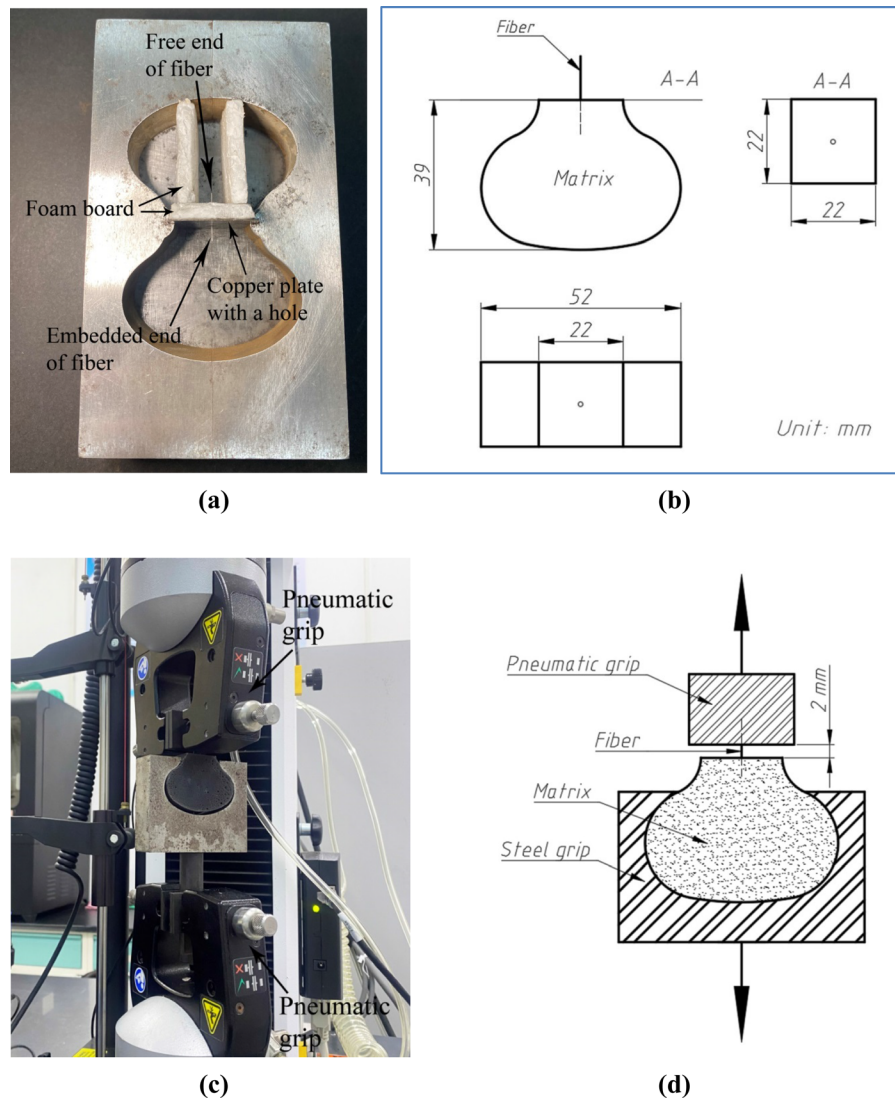
Fig. 2 **a** Placement of fiber prior casting specimen for fiber pullout test; **b** geometry of specimen for fiber pullout test; **c** setup for fiber pullout test; **d** scheme of fiber pullout test

the FA/C ratio increasing from 0 to 4. The incorporation of carbon black at a dosage of 2 or 10 kg/m^3 has little influence on the compressive strength. However, at a dosage up to 20 kg/m^3, carbon black obviously reduces the compressive strength. The matrices with 50% fly ash, i.e. the FA/C ratio is 1, and containing 2 or 10 kg/m^3 carbon black still exhibit a compressive strength higher than 80 MPa, falling in the category of high-strength concrete. The case with 80% fly ash and 20 kg/m^3 carbon black corresponds to the lowest compressive strength of 18.7 MPa. Accordingly, this specimen is of lightest weight with a density of

1320 kg/m^3. It is also clear from Table 4 that most specimens are light-weight with a density lower than 1800 kg/m^3.

From the viewpoint of fracture mechanics, the existence of defects with certain sizes and distribution in matrix favors a multiple-cracking process. Carbon black particles serve as defects which could reduce the fracture toughness of the matrix and facilitate the multiple-cracking and strain-hardening behavior of composites [29].

Table 4 Properties of matrices

Mix No	Spread (mm)	Density (kg/m³)	Compressive strength (MPa)
F0CB0	287	1880	94.0
F0CB2	281	1896	95.1
F0CB10	284	1893	83.5
F0CB20	279	1698	59.6
F1CB0	272	1665	83.4
F1CB2	276	1673	82.2
F1CB10	268	1656	75.2
F1CB20	268	1428	42.9
F2CB0	275	1526	73.5
F2CB2	274	1535	71.5
F2CB10	272	1580	62.4
F2CB20	271	1407	38.5
F4CB0	252	1442	34.6
F4CB2	254	1423	33.4
F4CB10	263	1408	27.6
F4CB20	245	1320	18.7

(a)   (b)
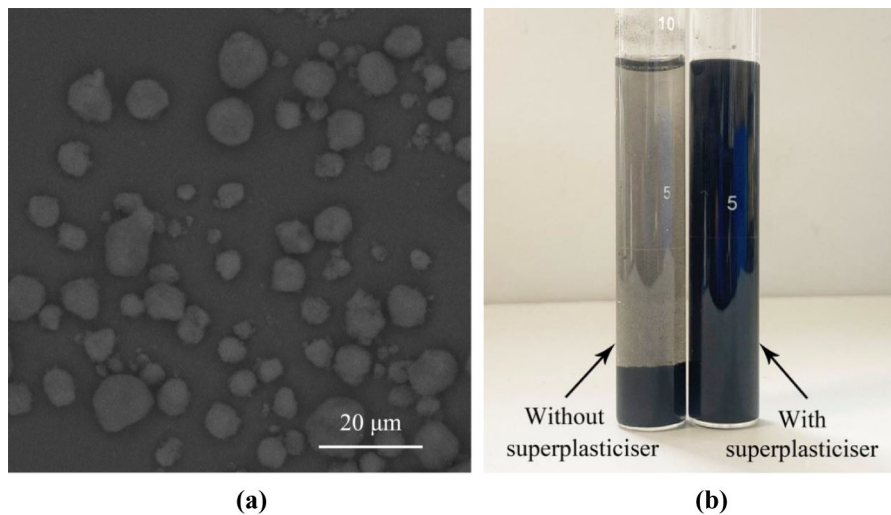
Fig. 3 **a** SEM images of carbon black; **b** carbon black particles in water without and with superplasticiser

3.3 Tensile properties

The stress–strain curves from direct tensile tests are given in Fig. 4. The salient values are listed in Table 5. The cracking patterns of the tensile specimens are shown in Fig. 5. It can be seen in Table 5 that the first-crack strength (σ_{tf}) ranges from 1.6 to 3.6 MPa, and the corresponding strain (ε_{tf}) from 0.03% to 0.09%. The ultimate strength (σ_{tu}) is in the range of 1.9–4.0 MPa, and the corresponding strain (ε_{tu}) 0.6–5.9%. It is clear from Fig. 4 that either the usage of fly ash or carbon black leads to the increase in the ultimate strain, but neither of them has a substantial individual effect. The ultimate strain for the composites containing fly ash without carbon black, i.e. F1CB0, F2CB0 and F4CB0, is still lower than 2%. For the composites containing carbon black but no fly ash, i.e. F0CB2, F0CB10 and F0CB20, the corresponding values are also smaller than 2%. For the composites containing both fly ash and carbon black, especially for the cases where their dosages were relatively high,
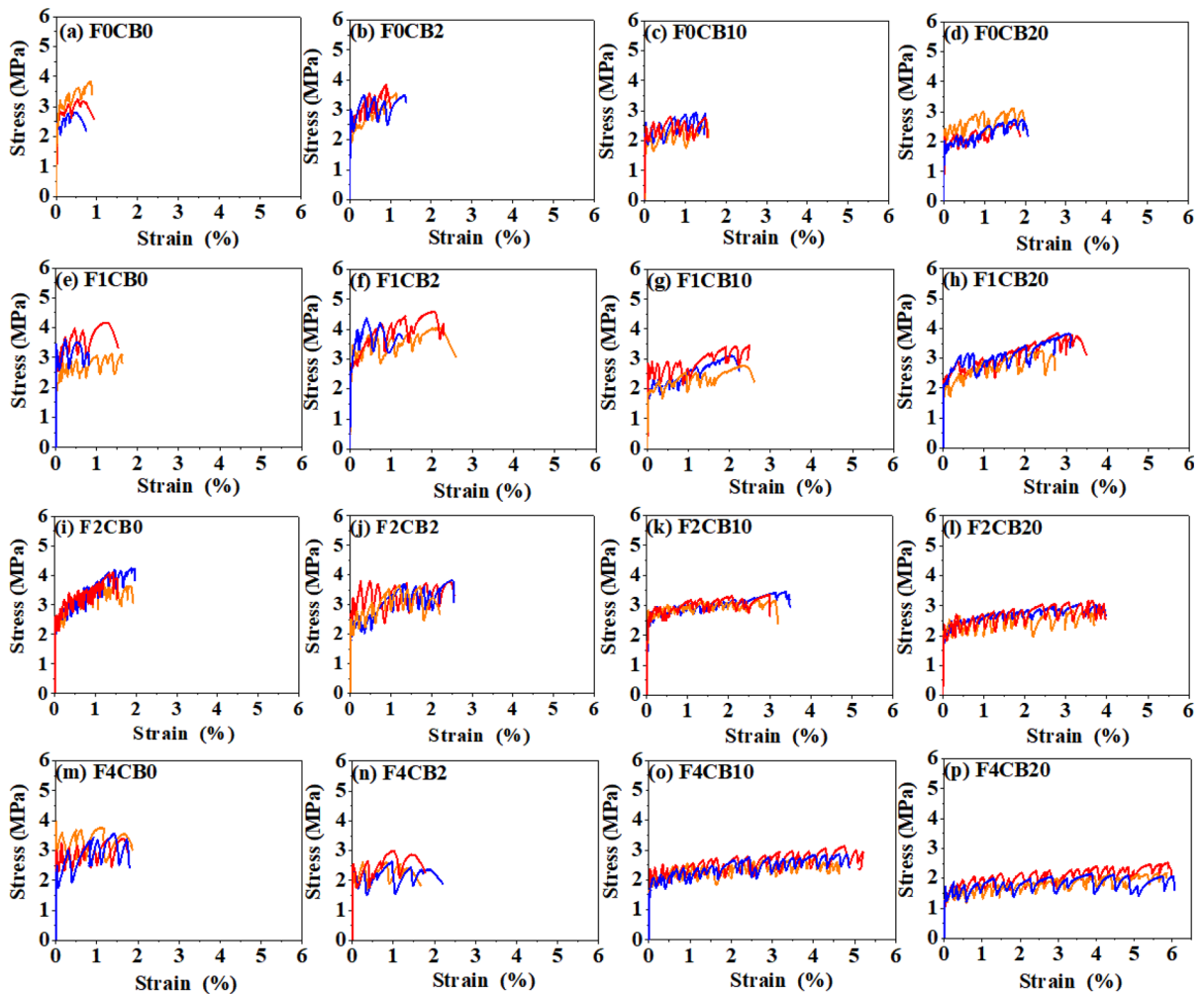
Fig. 4 Stress–strain curves from direct tensile tests

the ultimate strain increases immensely with the maximum value almost up to 6%.

It is also can be seen in Table 5 that the composites with a high dosage of carbon black tend to develop cracks with a relatively small width in general. At the FA/C ratio of 2 and with 10 or 20 g/m^3 carbon black, the composites exhibited the smallest crack widths, and the loaded and residual crack widths are lower than 0.20 and 0.10 mm, respectively.

Correspondingly, the multiple-cracking phenomenon becomes much more robust with the increase in the dosages of fly ash and carbon black, as can be seen from Fig. 5. For instance, only several cracks formed in F0CB0 composite containing neither fly ash nor carbon black. In contrast, a series of fine

cracks developed in F2CB20 and F4CB20 composites containing high dosages of fly ash and carbon black.

It should be noted that the compressive strength of the matrix for composite F2CB10 containing both fly ash and carbon black is 62.4 MPa, in comparison with 34.6 MPa for F4CB0 containing fly ash but no carbon black. The former displays an ultimate strain of 3.2% which is much high than 1.7% for the latter. This indicates that the increase in ductility of composites does not simply result from the reduction in matrix strength, and further confirms the coupling effect of fly ash and carbon black.

It can be also seen from Fig. 5 that the composites containing 10 or 20 g/m^3 carbon black have a large amount of small voids on their surface. It has been mentioned in Sect. 3.1 that a higher dosage of

Table 5 Tensile properties of SHCC at 28 days

Mix ID	σ_{tf} (MPa)	ε_{tf} (%)	σ_{tu} (MPa)	ε_{tu} (%)	Loaded crack width (mm)	Residual crack width (mm)
F0CB0	3.16	0.0826	3.64	0.6116	0.29	0.15
F0CB2	2.98	0.0652	3.24	1.1292	0.49	0.28
F0CB10	2.53	0.0561	2.67	1.5107	0.25	0.07
F0CB20	2.37	0.0369	2.35	1.8682	0.16	0.06
F1CB0	3.56	0.0820	3.59	1.2002	0.25	0.14
F1CB2	3.16	0.0705	3.49	1.8009	0.29	0.16
F1CB10	2.67	0.0644	3.22	2.2894	0.24	0.11
F1CB20	2.44	0.0360	3.03	3.0085	0.24	0.10
F2CB0	2.59	0.0738	3.98	1.7780	0.15	0.09
F2CB2	2.49	0.0625	3.63	2.3353	0.20	0.12
F2CB10	2.43	0.0534	3.42	3.2108	0.13	0.06
F2CB20	2.27	0.0366	2.71	3.8125	0.15	0.08
F4CB0	2.42	0.0666	3.34	1.6864	0.41	0.21
F4CB2	2.33	0.0571	2.77	1.5652	0.38	0.20
F4CB10	2.05	0.0364	2.52	4.8649	0.21	0.16
F4CB20	1.61	0.0324	1.98	5.9294	0.17	0.07

superplasticiser was adopted for the mixtures containing 10 or 20 g/m^3 carbon black. It is likely because more air was entrained by the high dosage of superplasticiser in these mixtures. The voids serve as defects which also enhance the multiple-cracking behavior.

The general status of the fibers at the crack planes was first observed at a low magnification under scanning electron microscope, as given in Fig. 6. It can be seen from Fig. 6 that the status of the fibers at the crack planes are affected by the presence of high dosages of fly ash and carbon black. For composites containing no or a relatively low dosages fly ash or carbon black, PVA fibers were mostly ruptured at the crack planes with a short pullout length. With the increase in the dosage of fly ash or carbon black, more PVA fibers tended to be pulled out completely without rupture with obviously longer pullout length. This trend is further confirmed by examining the fiber ends at a high magnification, as shown in Fig. 7. The ruptured fiber exhibits a tapering end, as shown in Fig. 7a, b, c, e, f and i. For the fibers pulled out completely, most of them experienced surface abrasion and damage as can be seen from Fig. 7d, g, h, j–l, and m–p).

It is worth mentioning that the fibers were mostly pulled out without rupture in all composites containing 80% fly ash, that is F4CB0, F4CB2, F4CB10 and F4CB20, but the corresponding ultimate strain values

for the former two are markedly lower than that for the latter two, as can be seen from Fig. 4. It is likely due to the fiber dispersing effect of carbon black at sufficient dosages. Carbon black particles tend to concentrate on the surface of PVA fibers and could facilitate the dispersion of PVA fibers. The non-oiled PVA fibers is easy to cluster due to hydrogen bonds formed between the hydroxyl groups on the surface of PVA fiber, which makes it difficult to evenly disperse non-oiled PVA fibers. It has been found that there are usually carboxyl and hydroxyl groups on the surface of carbon blacks [30]. Hence, carbon blacks have a tendency to be adsorbed on PVA fibers by hydrogen bonds, and impede the clustering of PVA fiber. In other words, the presence of sufficient carbon blacks favors an even dispersion of PVA fibers in the mixture. The mixtures of F4CB0 and F4CB2 had the relatively low flowability among all mixtures as can be seen from Table 4, which could be unfavorable for the dispersion of PVA fibers. Although mixture F4CB20 displayed even lower followability, the fibers could be well distributed under the dispersing effect of a high dosage of carbon black.

3.4 Fiber-matrix interfacial interactions

Due to its hydrophilic nature, non-oiled PVA fiber has a strong bond with cementitious matrix, and tends to
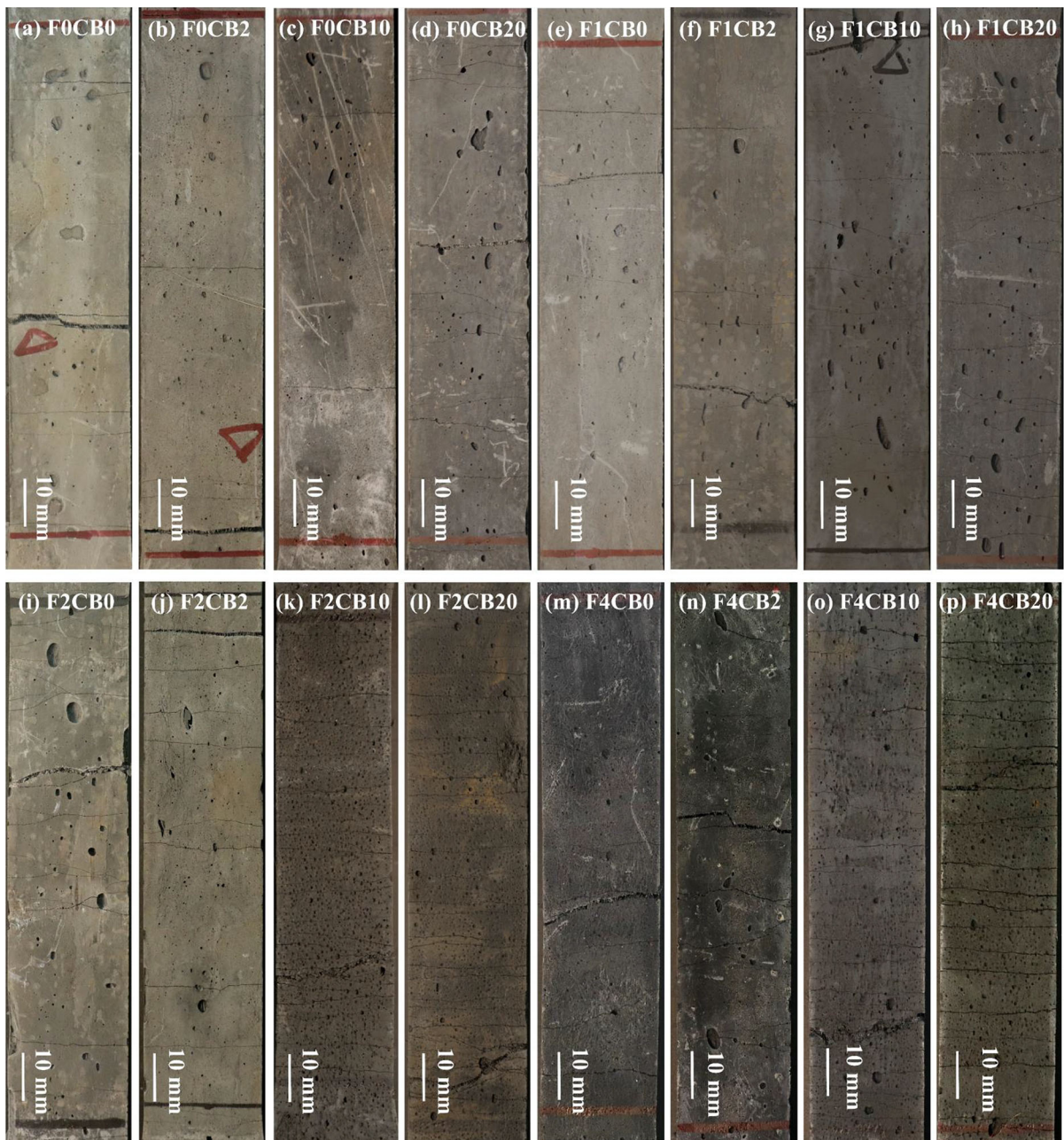
Fig. 5 Cracking patterns of specimens for direct tensile test

exhibit slip-hardening behavior in a fiber pullout test. The current experimental results indicate that the high dosages of fly ash and carbon black effectively reduce interfacial bond between non-PVA fiber and cementitious matrices, and lead to slip-softening behavior. More details are as follows.

The load–deflection curves from the fiber pullout tests are given in Fig. 8. The SEM observation on the embedded ends of the fibers after pullout testing is displayed in Fig. 9. The average fiber-matrix bond strength, chemical debonding energy, frictional bond strength and maximum tensile stress of the fiber are presented in Figs. 10.
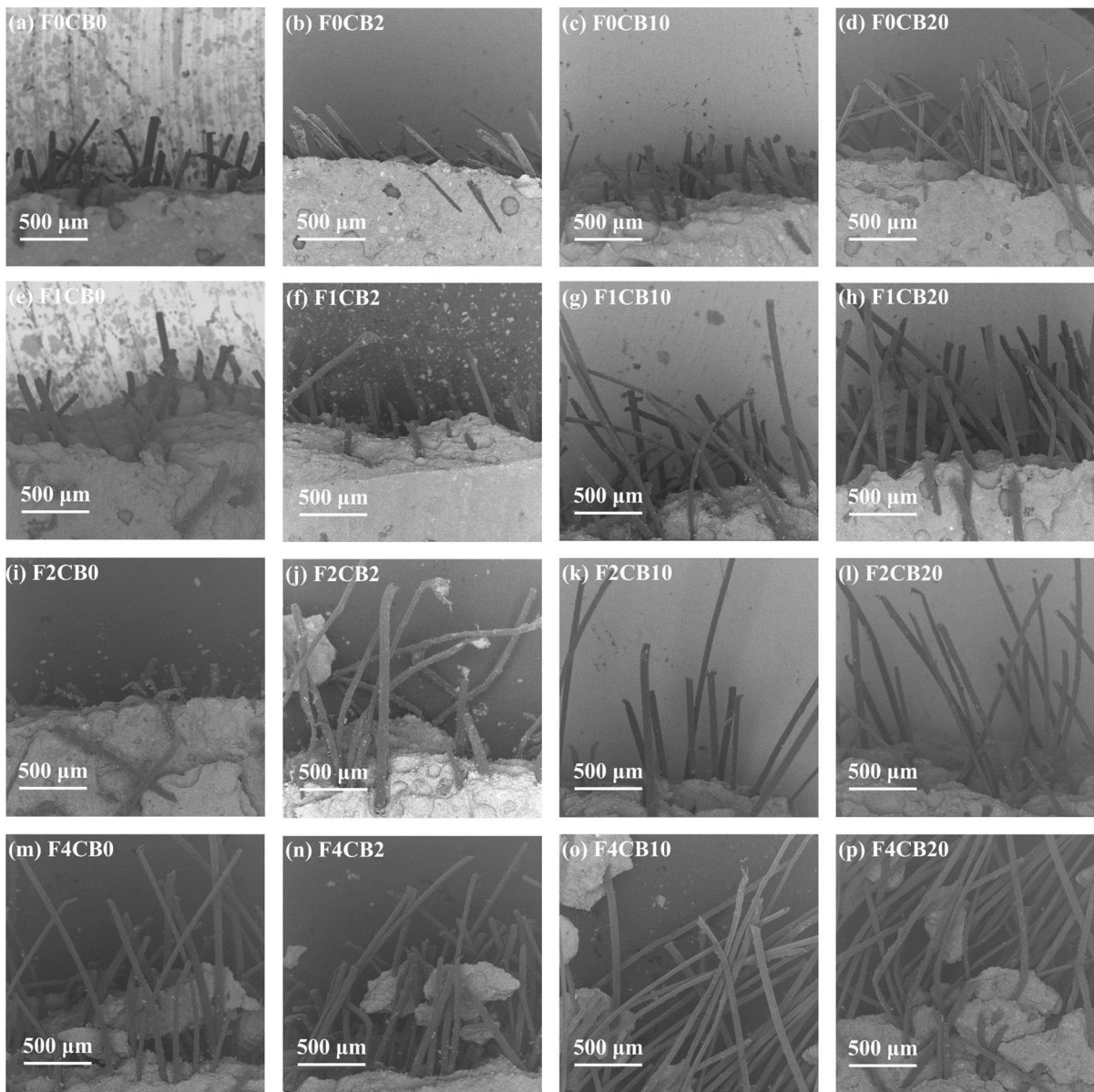
Fig. 6 SEM images of fibers at the cracking plane

The average bond strength is derived from the following formula:

$$\tau_{ave} = \frac{P_a}{\pi d_f l_e} \tag{2}$$

where P_a the maximum load of the linear branch of a load–displacement curve; d_f the fiber diameter and l_e the fiber embedment length. The bond strength herein is measurement of an average fiber-matrix interaction including both frictional and chemical bonds.

A fiber debonded/pullout model has been commonly used in analyzing the interfacial interactions between PVA fiber and cementitious matrices [31]. This model is adopted to calculate the chemical debonding energy, G_d, and frictional bond strength, τ_0, as shown in the following two equations
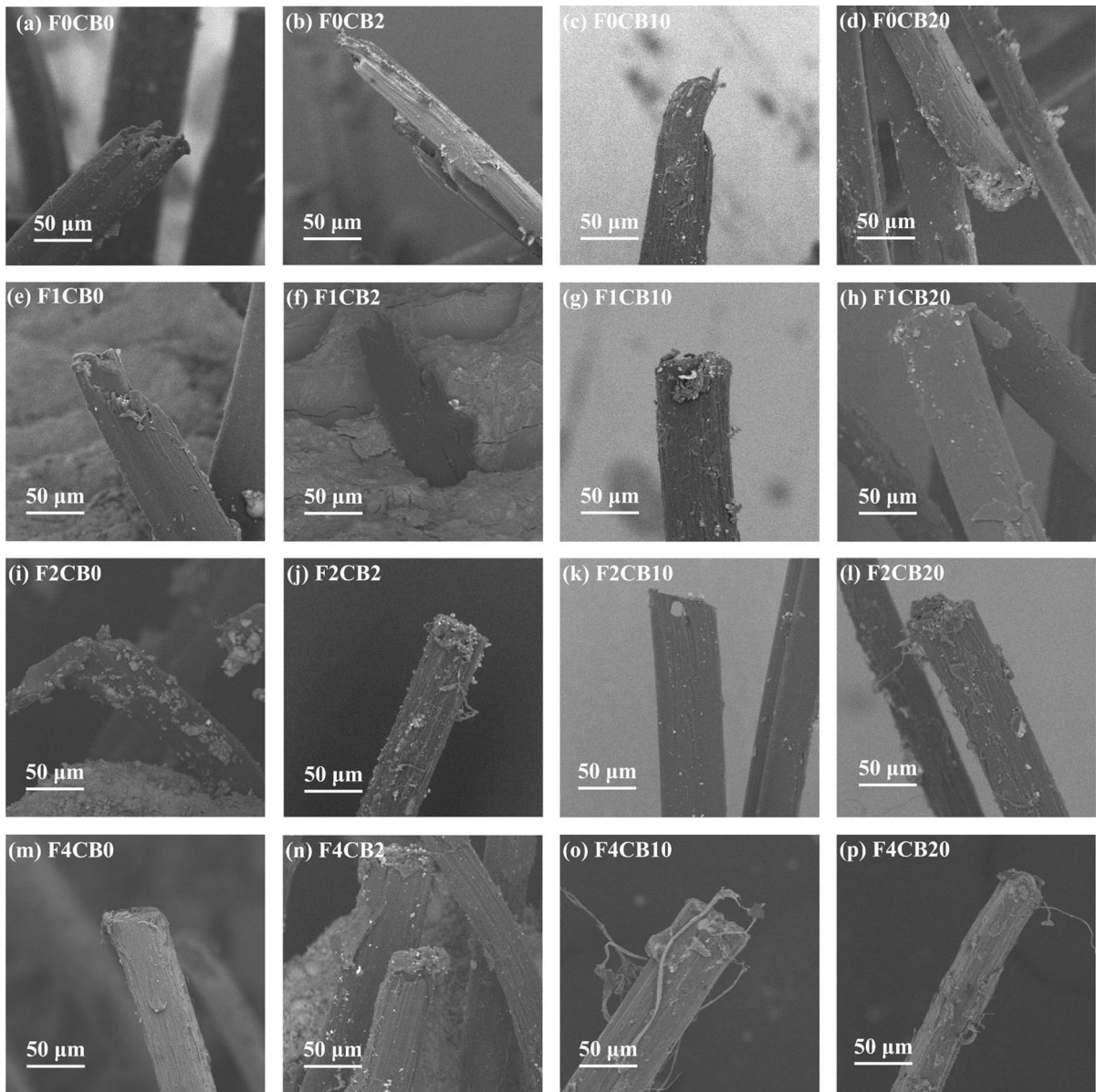
Fig. 7 SEM images of fiber ends at cracking plane

$$G_d = \frac{2(P_a - P_b)^2}{\pi^2 E_f d_f^3} \tag{3}$$

where E_f is the elastic modulus of fiber and P_b the load after sudden drop following P_a, and

$$\tau_0 = \frac{P_b}{\pi d_f l_e} \tag{4}$$

The maximum tensile stress of the fiber, σ_{max}, during the pullout test is derived from the maximum

load, P_{max}, over the whole pullout load–displacement curve, via the following equation:

$$\sigma_{max} = \frac{4P_{max}}{\pi d_f^2} \tag{5}$$

Note that P_a and P_{max} coincide for the case showing slip-softening behavior.

According to the results in Figs. 8 and 9, the pullout behavior of non-oiled PVA fiber can be classified in to three categories:
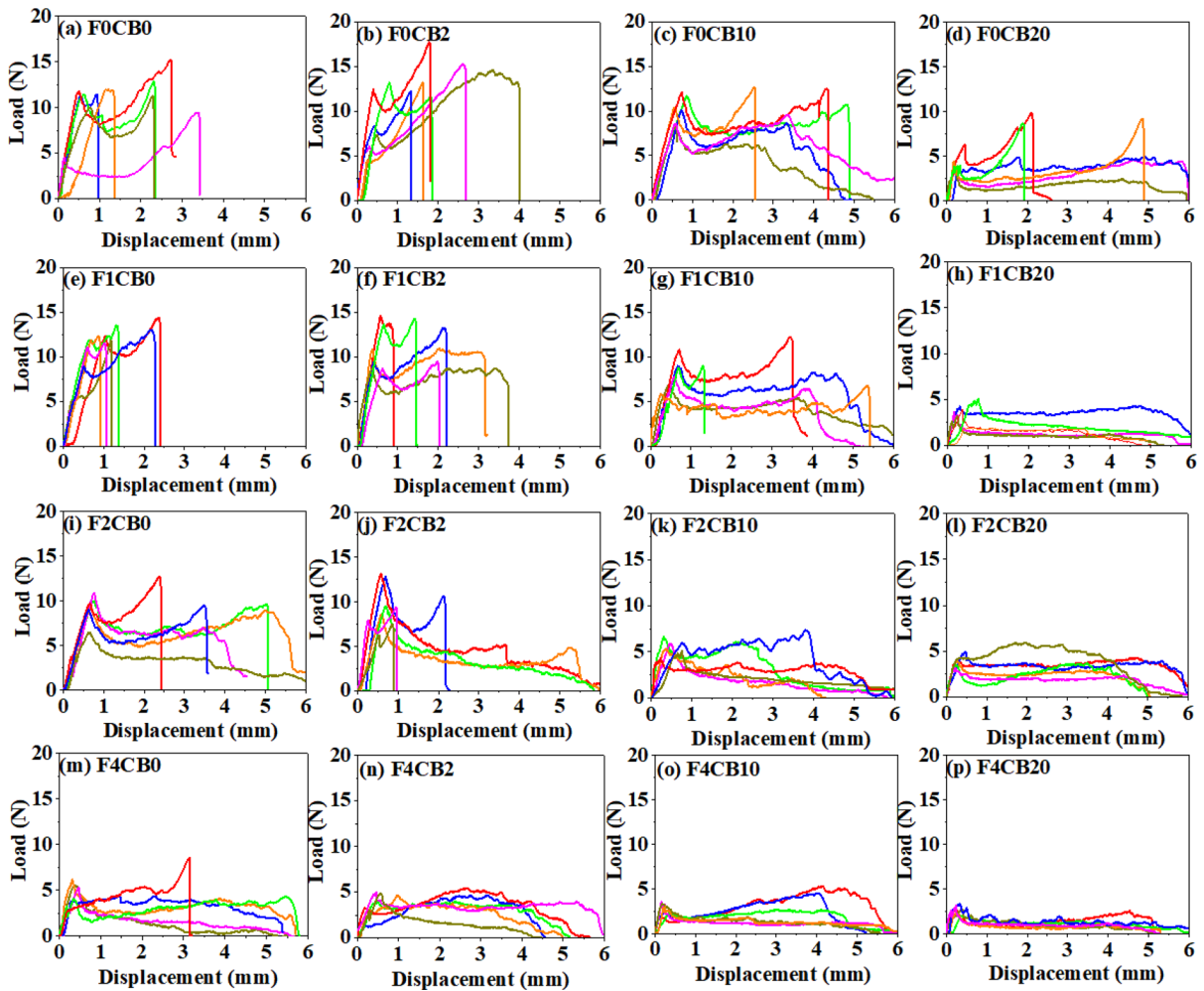
Fig. 8 Fiber pullout load–displacement curves

In the first category, the fiber is ruptured during most pullout tests. This category includes cases F0CB0, F0CB2, F1CB0 and F1CB2. As can be seen from Fig. 8a, b, e and f, the load–deflection curves display three phases: linear phase, slip-hardening phase, and a sudden load drop to zero at a displacement value lower than the embedded length 6 mm. Debonding occurs in the linear phase. The slip-hardening process is associated with the pulling-out process, where surface damage and delamination of the fiber happen as a result of fiber-matrix frictional interaction when sliding against the matrix. The sudden drop to zero in load, i.e., a complete loss of load carrying capacity, is associated with the fracture of the fiber. The rupture of fiber is confirmed by measuring the length of pullout segment. For the case

of fiber rupture, the pullout segment is shorter than the original embedment length. Also, it is further confirmed by SEM observation on the pullout segment. The fiber surface abrasion caused by fiber sliding against the matrix reduces the apparent strength of fiber [19]. That is why even though the fiber is ruptured in this category, the maximum tensile stress in the fiber as can be seen from Fig. 10d is lower than 1200 MPa, the tensile strength of the PVA fiber. Accordingly, the embedded ends of the fibers after pullout testing display tapering shape caused by fiber rupture, as shown in SEM images in Fig. 9a, b, e and f. This category presents strong interaction between non-oiled PVA fiber and matrices, with an average bond strength ranging from 3.39 to 3.89 MPa, a value in
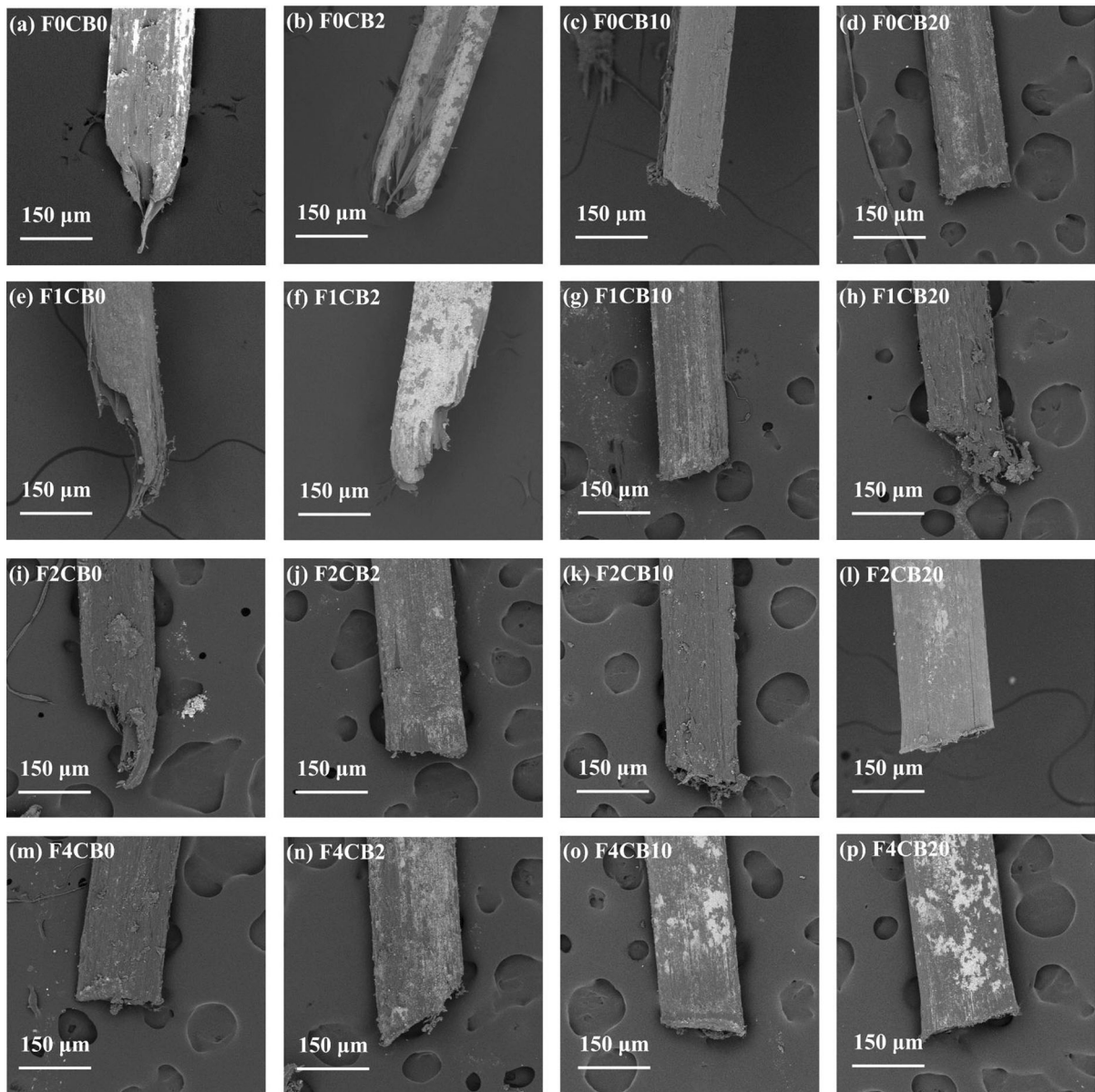
Fig. 9 SEM images of embedded ends of fibers after fiber pullout testing

chemical debonding energy 2.05–5.00 J/m^2, and a frictional bond strength 3.57–3.91 MPa.

In the second category, the fiber is pulled out completely without rupture for some specimens but fiber rupture occurs for others. This category covers cases F0CB10, F0CB20, F1CB10, F2CB0, F2CB2 and F4CB0. The corresponding average bond strength is within a range from 1.38 to 3.42 MPa, a value in chemical debonding energy 0.51–3.03 J/m^2, and a

frictional bond strength 1.30–3.56 MPa, referred to as medium bond strength.

In the third category, the fiber is pulled out completely without rupture. Cases F1CB20, F2CB10, F2CB20, F4CB2, F4CB10 and F4CB20 belong to this category, with a relatively low average bond strength ranging from 0.95 to 1.96 MPa, a value in chemical debonding energy 0.24–0.77 J/m^2, and a frictional bond strength 0.94–1.96 MPa. For all
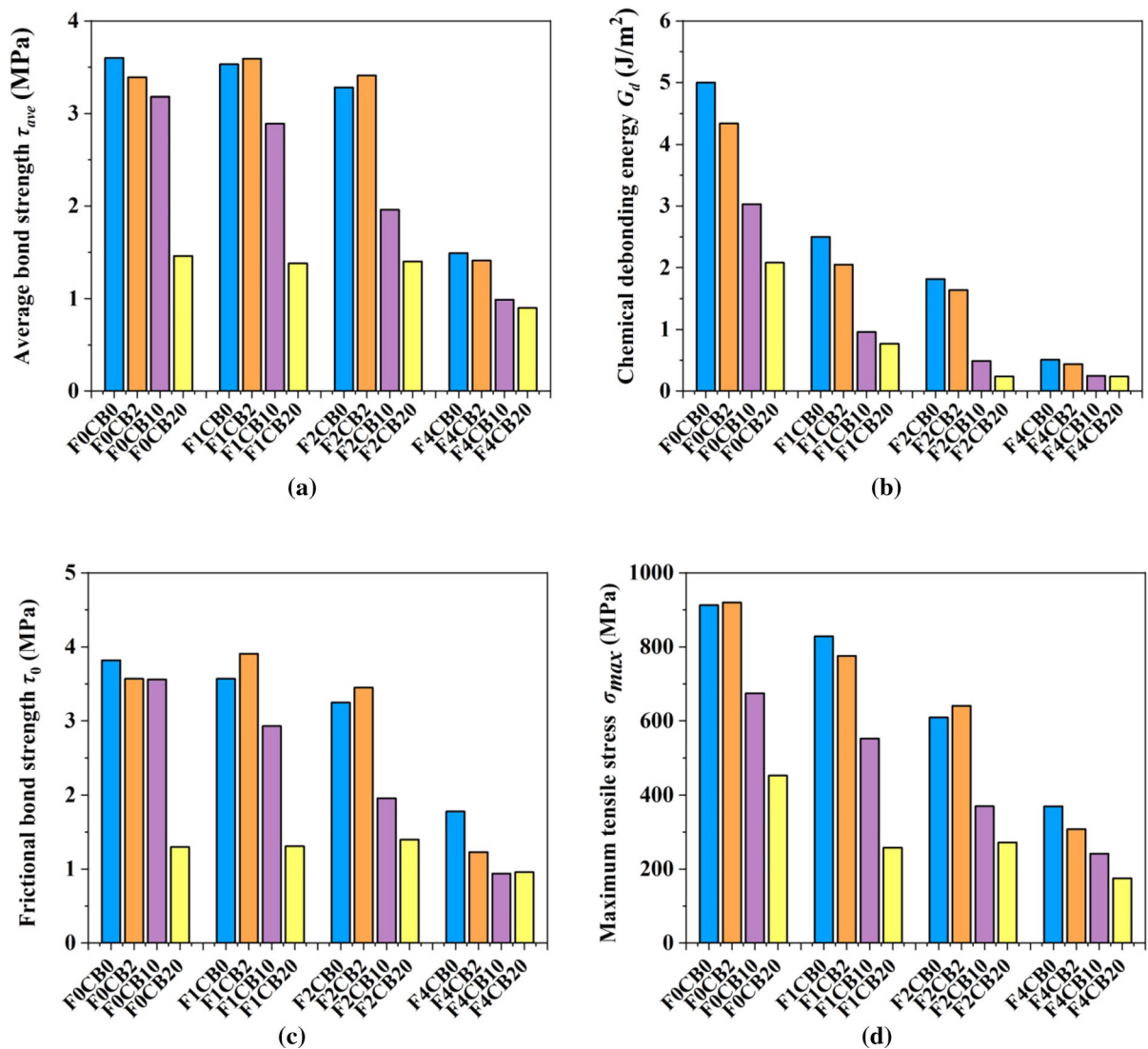
Fig. 10 **a** Average bond strength between PVA fiber and matrices; **b** chemical debonding energy; **c** frictional bond strength; **d** maximum tensile stress of PVA fiber during fiber pullout test

specimens in this category, the fiber is pulled out without rupture.

It can be seen from Fig. 8 that both the fly ash and carbon black tend to reduce the interfacial interaction between the non-oiled PVA fiber and the cementitious matrix. As a result, the fiber pullout behavior generally transform from the first category to the third category with the increase in the dosages of fly ash and carbon black, with the second category as a transition. For instance, in the matrix F0CB0 that contains neither fly ash nor carbon black, the PVA fiber exhibits the fiber pullout behavior of the first category. The

incorporation of carbon black at a dosage of 2 kg/m^3 has little influence on the pullout behavior of the fiber. However, with the dosage of carbon increased to 10 kg/m^3, the fiber pullout behavior displays features of the second category. There are 3 out 6 specimens giving a slowly declining slip-softening branch in load–displacement curves. SEM observation as presented in Fig. 9c confirmed that the fibers were pulled out without rupture, but with substantial surface abrasion and delamination.

Note that the flat end of the fiber is left by cutting a long filament into short fibers during the fiber

manufacture process. For the other 3 cases, the load–displacement curves still end with a sudden drop, and the fibers were ruptured. It is likely that these 3 cases experienced larger snubbing effect which causes the rupture of the fiber. It should be noted that to an extent subbing effect is involved in fiber pullout tests considering that the perfect alignment of fiber is rarely possible in real-life situations. It has been reported that PVA fiber experiences subbing effect at the exit point of the matrix when the obliquely aligned fiber pulls out from the matrix [19].

For high-strength matrices of a compressive strength of higher than 80 MPa, including F0CB0, F0CB2, F1CB0, F1CB2 and F0CB10, the former four have such strong interactions with PVA fiber that the fibers were fractured which was confirmed by SEM observation as shown in Fig. 9a, b, e and f. In F0CB10 matrix that contains 10 kg/m^3 carbon black, the PVA fiber can be pulled out completely without rupture. This indicates that carbon black at a dosage of 10 kg/m^3 effectively reduces the interfacial bond of non-oiled PVA fiber and cementitious matrix while maintaining high strength of the composite. The interfacial bond was reduced further with the dosage of carbon black increased to 20 kg/m^3, which also reduced markedly the compressive strength.

It is worth mentioning that the low bonding strength does not simply result from low strength of the matrix. It has been indicated in Table 4 that the matrix strength of F2CB20 is higher than that of F4CB0, but the corresponding bond strength of the former is lower than that of the latter as can be seen from Fig. 10a. The former contains 20 kg/m^3, in contrast to no carbon black in the latter. Hence, this is largely due to the role of carbon black in reducing interfacial interaction. This can be further supported by similar comparison between cases F0CB10 and F1CB0. The former is of slightly higher compressive strength than the latter, but the corresponding bond strength for the former is lower.

On the one hand, the hydrophobic nature of carbon black could contribute to the reduction of the bond between PVA fiber and cementitious matrix. On the other hand, the spherical shape and the lubricant effect of carbon black particles could lessen the sharp angles of the matrix and alleviate the surface abrasion when the fiber is sliding against the matrix. It has been reported that PVA fibers tend to be peeled off when sliding against the contacting cementitious matrix

during the pullout process [2]. Both the spherical shape and lubricant effect of carbon black could reduce the surface abrasion of PVA fibers. Furthermore, fly ash also contains spherical particles and residual carbon from incomplete combustion. It is likely that fly ash also has a similar lubricating effect [26]. Hence, non-oiled PVA fibers are more likely to be pulled out completely without rupture in the cementitious matrices containing high dosages of carbon black and fly ash. Ultra-ductile SHCC can be produced with non-oiled PVA fibers under the coupling effect of carbon black and fly ash.

4 Conclusions

Ultra-ductile SHCC with an ultimate strain of almost 6% has been developed by using non-oil-coated PVA fibers together with high contents of fly ash and carbon black. By varying the contents of fly ash and carbon black along with the dosage of the superplasticiser, cementitious matrices with compressive strengths suitable for designing SHCC with PVA fibers have been obtained. The intensity of multiple-cracking and strain-hardening behavior generally increases with the contents of fly ash and carbon black. The bond between non-oiled PVA fibers and cementitious matrices has been sufficiently reduced by the coexistence of fly ash and carbon black, and therefore the premature fracture of PVA fibers has been prevented. The coupling effect of fly ash and carbon black has improved the performance of non-oiled PVA fibers in SHCC in terms of ductility. By using carbon black along with fly ash and non-oiled PVA fibers, it not only reduces the production costs, but could also enhance the conductivity and self-sensing ability of SHCC. It can be expected that this SHCC could find various applications in buildings and transportation such as self-sensing wall, bridge deck and tunnel linings.

Availability of data and materials All data necessary to reproduce the results in this study are available from the corresponding author on request.

Code availability Not applicable.

Declarations

Conflict of interest   The authors have no conflicts of interest to disclose.

Ethical approval   Not applicable.

Consent to participate   Not applicable.

Consent for publication   Not applicable.

References

1. Li VC, Wang SX, Wu C (2001) Tensile strain-hardening behavior of polyvinyl alcohol engineered cementitious composite (PVA-ECC). ACI Mater J 98:483–492. https://doi.org/10.14359/10851
2. Li VC, Wu C, Wang SX, Ogawa A, Saito T (2002) Interface tailoring for strain-hardening polyvinyl alcohol engineered cementitious composite (PVA-ECC). ACI Mater J 99:463–472. https://doi.org/10.14359/12325
3. Wille K, Kim DJ, Naaman AE (2011) Strain-hardening UHP-FRC with low fiber contents. Mater Struct 44:583–598. https://doi.org/10.1617/s11527-010-9650-4
4. Yang EH, Li VC (2012) Tailoring engineered cementitious composites for impact resistance. Cem Concr Res 42:1066–1071. https://doi.org/10.1016/j.cemconres.2012.04.006
5. Sahmaran M, Ozbay E, Yucel HE, Lachemi M, Li VC (2012) Frost resistance and microstructure of engineered cementitious composites: influence of fly ash and micro poly-vinyl-alcohol fiber. Cem Concr Compos 34:156–165. https://doi.org/10.1016/j.cemconcomp.2011.10.002
6. Yang YZ, Lepech MD, Yang EH, Li VC (2009) Autogenous healing of engineered cementitious composites under wet-dry cycles. Cem Concr Res 39:382–390. https://doi.org/10.1016/j.cemconres.2009.01.013
7. Kan LL, Shi HS (2012) Investigation of self-healing behavior of Engineered Cementitious Composites (ECC) materials. Constr Build Mater 29:348–356. https://doi.org/10.1016/j.conbuildmat.2011.10.051
8. Leung CKY, Cao QA (2010) Development of pseudo-ductile permanent formwork for durable concrete structures. Mater Struct 43:993–1007. https://doi.org/10.1617/s11527-009-9561-4
9. Li VC, Leung CKY (1992) Steady-state and multiple cracking of short random fiber composites. J Eng Mech-ASCE 118:2246–2264. https://doi.org/10.1061/(ASCE)0733-9399(1992)118:11(2246)
10. Li VC, Wu HC (1992) Conditions for pseudo strain-hardening in fiber reinforced brittle matrix composites. Appl Mech Rev 45:390–398. https://doi.org/10.1115/1.3119767
11. Naaman AE (2003) Enigeered steel fibers with optimal properties for reinforcement of cement composites. J Adv Concr Technol 1:241–252. https://doi.org/10.3151/jact.1.241
12. Zhang Y, Sun W, Shang L, Pan G (1997) The effect of high content of fly ash on the properties of glass fiber reinforced cementitious composites. Cem Concr Res 27:1885–1891. https://doi.org/10.1016/S0008-8846(97)00203-2
13. Kayali O (2004) Effect of high volume fly ash on mechanical properties of fiber reinforced concrete. Mater Struct 37:318–327. https://doi.org/10.1007/BF02481678
14. Wu J-D, Guo L-P, Cao Y-Z, Lyu B-C (2022) Mechanical and fiber/matrix interfacial behavior of ultra-high-strength and high-ductility cementitious composites incorporating waste glass powder. Cem Concr Compos 126:104371. https://doi.org/10.1016/j.cemconcomp.2021.104371
15. Lin C, Kayali O, Morozov EV, Sharp DJ (2014) Influence of fibre type on flexural behaviour of self-compacting fibre reinforced cementitious composites. Cem Concr Compos 51:27–37. https://doi.org/10.1016/j.cemconcomp.2014.03.007
16. Lin C, Kayali O, Morozov EV, Sharp DJ (2017) Development of self-compacting strain-hardening cementitious composites by varying fly ash content. Constr Build Mater 149:103–110. https://doi.org/10.1016/j.conbuildmat.2017.05.051
17. Arain MF, Wang M, Chen J, Zhang H (2019) Study on PVA fiber surface modification for strain-hardening cementitious composites (PVA-SHCC). Constr Build Mater 197:107–116. https://doi.org/10.1016/j.conbuildmat.2018.11.072
18. Ding C, Guo L, Chen B, Xu Y, Cao Y, Fei C (2019) Micromechanics theory guidelines and method exploration for surface treatment of PVA fibers used in high-ductility cementitious composites. Constr Build Mater 196:154–165. https://doi.org/10.1016/j.conbuildmat.2018.11.118
19. Kanda T, Li VC (1998) Interface property and apparent strength of high-strength hydrophilic fiber in cement matrix. J Mater Civil Eng 10:5–13. https://doi.org/10.1061/(ASCE)0899-1561(1998)10:1(5)
20. Pan Z, Wu C, Liu J, Wang W, Liu J (2015) Study on mechanical properties of cost-effective polyvinyl alcohol engineered cementitious composites (PVA-ECC). Constr Build Mater 78:397–404. https://doi.org/10.1016/j.conbuildmat.2014.12.071
21. Zhang Z, Zhang Q (2018) Matrix tailoring of Engineered Cementitious Composites (ECC) with non-oil-coated, low tensile strength PVA fiber. Constr Build Mater 161:420–431. https://doi.org/10.1016/j.conbuildmat.2017.11.072
22. Cui H, Jin Z, Zheng D, Tang W, Li Y, Yun Y, Lo TY, Xing F (2018) Effect of carbon fibers grafted with carbon nanotubes on mechanical properties of cement-based composites. Constr Build Mater 181:713–720. https://doi.org/10.1016/j.conbuildmat.2018.06.049
23. Huang Y, Li H, Qian S (2018) Self-sensing properties of Engineered Cementitious Composites. Constr Build Mater 174:253–262. https://doi.org/10.1016/j.conbuildmat.2018.04.129
24. Deng H, Li H (2018) Assessment of self-sensing capability of Carbon Black Engineered Cementitious Composites. Constr Build Mater 173:1–9. https://doi.org/10.1016/j.conbuildmat.2018.04.031
25. Yıldırım G, Öztürk O, Al-Dahawi A, Afşın Ulu A, Şahmaran M (2020) Self-sensing capability of Engineered Cementitious Composites: effects of aging and loading

conditions. Constr Build Mater 231:117132. https://doi.org/10.1016/j.conbuildmat.2019.117132

26. Wang SX, Li VC (2007) Engineered cementitious composites with high-volume fly ash. ACI Mater J 104:233–241. https://doi.org/10.1201/b15883-8

27. Kim JK, Kim JS, Ha GJ, Kim YY (2007) Tensile and fiber dispersion performance of ECC (engineered cementitious composites) produced with ground granulated blast furnace slag. Cem Concr Res 37:1096–1105. https://doi.org/10.1016/j.cemconres.2007.04.006

28. Zhou J, Qian SZ, Beltran MGS, Ye G, van Breugel K, Li VC (2010) Development of engineered cementitious composites with limestone powder and blast furnace slag. Mater Struct 43:803–814. https://doi.org/10.1617/s11527-009-9549-0

29. Yao Y, Zhu Y, Yang YZ (2012) Incorporation superabsorbent polymer (SAP) particles as controlling pre-existing flaws to improve the performance of engineered cementitious composites (ECC). Constr Build Mater 28:139–145. https://doi.org/10.1016/j.conbuildmat.2011.08.032

30. Donnet JB (1982) Structure and reactivity of carbons: from carbon black to carbon composites. Carbon 20:267–282. https://doi.org/10.1016/0008-6223(82)90002-1

31. Redon C, Li VC, Wu C, Hoshiro H, Saito T, Ogawa A (2001) Measuring and modifying interface properties of PVA fibers in ECC matrix. J Mater Civ Eng 13:399–406. https://doi.org/10.1061/(ASCE)0899-1561(2001)13:6(399)